Improving sea ice thickness estimates by assimilating CryoSat-2 and SMOS sea ice thickness data simultaneously

Longjiang Mu[a], Qinghua Yang[a]*, Martin Losch[b], Svetlana N. Losa[b,c], Robert Ricker[b], Lars Nerger[b], Xi Liang[a]

a. Key Laboratory of Research on Marine Hazards Forecasting, National Marine Environmental Forecasting Center, Beijing, China
b. Alfred Wegener Institute, Helmholtz Centre for Polar and Marine Research, Bremerhaven, Germany
c. St. Petersburg Department of P. P. Shirshov Institute of Oceanology, St. Petersburg, Russia

Correspondence to: Q. Yang, National Marine Environmental Forecasting Center, Dahuisi 8, 100081, Beijing, China. E-mail: yqh@nmefc.gov.cn

Abstract

The impact of assimilating weekly CryoSat-2 sea ice thickness data together with daily SMOS sea ice thickness and daily SSMIS sea ice concentration data on the sea ice fields of a coupled sea ice-ocean model of the Arctic Ocean is investigated. The sea-ice model is based on the Massachusetts Institute of Technology general circulation model (MITgcm) and the assimilation is performed by a localized Singular Evolutive Interpolated Kalman (LSEIK) filter coded in the Parallel Data Assimilation Framework (PDAF). A period of three months from 1 November 2011 to 30 January 2012 is selected to assess the skill of the assimilation system in the cold season. Compared to the unassimilated solution and a solution where only sea ice concentration is assimilated, the model-data misfits are substantially reduced in areas of both thick and thin ice. The sea ice thickness estimates agrees significantly better with in situ observations in the central Arctic Ocean than the sea ice thickness obtained from assimilating SMOS data alone, while the sea ice concentration shows very small improvements. The sea ice fields obtained by the joint assimilation of SMOS and CryoSat-2 data also have lower errors in thickness and concentration than those obtained from directly assimilating a statistically merged SMOS and CryoSat-2 sea ice thickness product. These lower errors suggest that model dynamics play a significant role in data blending.

Key Words: data assimilation; ensemble Kalman filter; sea ice thickness; CryoSat-2; SMOS; Arctic

1. Introduction

State of the art sea ice models rely on parameterizations for many physical processes. To minimize the uncertainties of model predictions especially for short-term forecasts, sea ice concentration data have been assimilated into coupled sea ice-ocean models by different assimilation methods (Lisæter et al., 2003; Lindsay and Zhang, 2006; Stark et al., 2008; Massonnet et al., 2013; Yang et al., 2015). Day et al. (2014) showed accurate sea ice thickness initialization to be also important for summer sea ice concentration and extent forecasts. There are, however, only a few studies addressing the topic of ice thickness data assimilation, because (1) the in situ observations of sea ice thickness are sparse in space and time, (2) satellite measurements from which basin-scale Arctic sea ice thickness can be derived are only available for the last decade, and (3) the processing of the data is still a field of ongoing research (Ricker et al., 2014, 2017). For example, Lisæter et al. (2007) demonstrated the importance of ice thickness assimilation on sea ice variables and ocean fields in a coupled sea ice-ocean model in a study with an ensemble Kalman filter and synthetic CryoSat sea ice thickness data. Yang et al. (2014) assimilated the near-real-time Soil Moisture Ocean Salinity (SMOS) satellite-based sea ice thickness data (Tian-Kunze et al., 2014) into a coupled ice-ocean model using an ensemble-based localized singular evolutive interpolated Kalman (LSEIK) filter (Pham et al., 1998; Nerger et al., 2006). However, the SMOS sea ice thickness retrieval is only applicable for thin ice (< 1 m) (Tian-Kunze et al., 2014). The impact of SMOS sea ice thickness was further investigated during both the early melting and freezing seasons (Xie et al., 2016). Both Yang et al. (2014) and Xie et al. (2016) showed that assimilating SMOS ice thickness strongly improves simulated first-year ice, while thick (multi-year) ice was not significantly improved.

The European Space Agency (ESA) satellite mission CryoSat-2, launched in 2010, is dedicated to obtaining the thickness of perennial sea ice (Wingham et al., 2006). Regularly updated CryoSat-2 thickness data products (Laxon et al., 2013;

Ricker et al., 2014; Tilling et al., 2015) now allow studies of interannual changes in the thick ice area and, moreover, serve for climate modelling studies. These thickness data are derived from radar altimetry measurements that are used to derive sea ice freeboard, the height of the ice surface above the water level. Freeboard is then converted into sea ice thickness, assuming hydrostatic equilibrium and employing an effective approach on snow loading (Laxon et al., 2013). Due to the larger freeboard of thick ice, better performance is expected for multi-year sea ice thickness (Ricker et al., 2014), so that SMOS data and CryoSat-2 data complement each other. The novel CryoSat-2 thickness data provide a good opportunity to investigate the impact of assimilating multi-year ice thickness on the quality of sea ice reanalysis.

The two complementary datasets were recently combined with an optimal interpolation scheme (Ricker et al., 2017). This combined CS2SMOS dataset covers both thin ice and thick ice in the Arctic. However, optimal interpolation is a purely statistical method that does not take into account any physical processes.

We extend the study of Yang et al. (2016) with the aim to improve 24h-forecasts of perennial sea ice thickness. To achieve this, the weekly averaged CryoSat-2 ice thickness is assimilated into our forecasting system in addition to the Special Sensor Microwave Imager Sounder (SSMIS) sea ice concentration and SMOS sea ice thickness data (Yang et al., 2016). To account for atmospheric uncertainties we follow Yang et al. (2015, 2016) and use the same ensemble atmospheric forcing from the THORPEX Interactive Grand Global Ensemble (TIGGE) dataset (Park et al., 2008; Bougeault et al., 2010). The same autumn-winter seasonal transition period from 1 November 2011 to 30 January 2012 is chosen to simplify comparisons with Yang et al. (2015, 2016). To assess the role of model dynamics in data blending we further compare the performance of the forecasting system assimilating SMOS and CryoSat-2 datasets individually with the combined CS2SMOS data product and the results of assimilating the CS2SMOS dataset directly.

The paper is organized as follows: In section 2, the model and atmospheric forcing are described. Further, the data assimilation method and the observational data used for the assimilation and evaluation are introduced. In addition, the configurations of each experiment are shown. In section 3, the assimilation experiments are evaluated. The role of model dynamics in data blending is discussed in section 4.

Conclusions of this study are made in section 5.

2. **Forecasting system**

2.1. Model description

The forecasting system uses the Massachusetts Institute of Technology general circulation model (MITgcm, Marshall et al., 1997). The Arctic regional configuration has been widely used to study both sea ice and oceanic processes (Losch et al., 2010; Nguyen et al., 2011; Mu et al., 2017). The sea ice dynamics uses a viscous plastic rheology (Hibler, 1979; Zhang and Hibler, 1997), the thermodynamics follows Parkinson and Washington (1979) with a one-layer, zero heat capacity formulation. To allow ice growth also for thick ice, there are 7 thickness categories with a prescribed homogenous distribution between 0 and 2h (h = mean thickness, averaged over the ice covered part of the grid cell) that is scaled with the mean ice thickness (Hibler, 1984). In this way, there is always thin ice of thickness (2/7)h available. Note that the mean sea ice thickness of the model output in the paper is the grid-cell mean thickness (i.e. thickness weighted by concentration). Snow is treated following Zhang et al. (1998) and snow thickness is an additional prognostic variable that moves with the ice. The same 7-thickness-category distribution is also used for snow. This parameterization usually leads to thicker sea ice (up to 1 m) and reduces a thin ice bias in the model (Castro-Morales et al., 2014). Arakawa C grids are used for both the ocean and sea ice with an average spacing of approximately 18 km. Model parameters for sea ice and ocean were optimized by Nguyen et al. (2011). The model resolves near surface processes with 28 unevenly spaced layers in the top 1000 m and 22 thicker, but also unevenly spaced, layers below 1000 m. The bathymetry is derived from the National Centers for Environmental Information (formerly the National Geophysical Data Center (NGDC)) 2-minute gridded elevations/bathymetry for the world (ETOPO2; Smith and Sandwell, 1997). Monthly oceanic boundary conditions for the Atlantic and Pacific sections are provided by a global model with the same horizontal resolution (~18 km) as the regional model (Menemenlis et al., 2008). The monthly mean river runoff is based on the Arctic Runoff Data Base (ARDB) as prepared by P. Winsor (Nguyen et al., 2011). For more details of the model configuration the reader is referred to Losch et al. (2010) and Nguyen et al. (2011).

2.2. Atmospheric forcing

Following Yang et al. (2016), the same model is forced by atmospheric ensemble forecasts of the UK Met Office Unified Model (UKMO; Bowler et al., 2008) available in the TIGGE archive (http://tigge.ecmwf.int). 23 sets of perturbed forecasts' fields are used to force 23 ensemble members of the model states for an approximation of the forecast error statistics, so that there is no need for any additional ensemble inflation. The reader is referred to Yang et al. (2015) for more details on data processing for the model.

2.3. Data preparation

Observations of sea ice concentration used for assimilation are provided by the NSIDC (http://nsidc.org/data/docs/daac/nsidc0051_gsfc_seaice.gd.html). They are derived from Defense Meteorological Satellite (DMSP) F17 SSMIS passive microwave data using the NASA team algorithm (Cavalieri et al., 2012). The daily sea ice concentration data are provided in polar stereographic projection at a grid cell size of 25 × 25 km, and are then linearly interpolated onto the model grid. Following Yang et al. (2016), a uniform constant value of 0.25 is used as observation error to account for measurement and representation errors (Janjić et al., 2017).

For sea ice thicknesses below 1.0 m, observational data have been derived from the SMOS brightness temperatures (Tian-Kunze et al., 2014; http://icdc.zmaw.de, version 2). The sea ice thickness data have a horizontal grid resolution of 12.5 km. They are interpolated onto the model grid and then assimilated into the forecasting system following Yang et al. (2014). The data assimilation uses the uncertainties provided by this daily product as assumed observation errors.

To improve thick sea ice estimates, sea ice thickness data derived from CryoSat-2 radar altimetry measurements (Ricker et al., 2014; http://data.meereisportal.de/data, version 1.2) are assimilated in addition to the SMOS data. The CryoSat-2 sea ice thickness retrievals are provided as weekly means, projected onto the EASE-Grid 2.0 (Brodzik et al., 2012) with a grid resolution of 25 km. The estimated thickness uncertainties provided in the dataset are also used directly in the data assimilation. Both, the CryoSat-2 ice thickness data and its uncertainties are interpolated onto the model grid. For synchronization with the daily availability of the SSMIS-derived sea ice concentration and SMOS-derived sea ice thickness, the weekly mean sea ice thickness data from CryoSat-2 are assimilated every day of the week.

The complementary character of the uncertainties of the observed thickness ranges of the two datasets makes it possible to combine the weekly CryoSat-2 and daily SMOS data with an optimal interpolation scheme into a merged product (CS2SMOS), which covers the entire thickness range (Ricker et al., 2017; http://data.meereisportal.de/data). The data merging is carried out on a weekly basis to accommodate the different temporal resolutions of the individual retrievals. While SMOS obtains Arctic-wide thin ice thickness within a day, CryoSat-2 data do not provide full Arctic coverage and need to be collected over one month to retrieve a full coverage of the Arctic. The CS2SMOS sea ice thickness data provide a full coverage of the Arctic domain including the North Pole, and are projected onto the 25 km EASE-Grid 2.0. For the data assimilation, the CS2SMOS sea ice thickness data and its uncertainties are interpolated onto the model grid. The weekly CS2SMOS data are assimilated every day of the week as the CryoSat-2 data.

To assess the model skill in 24-hour predictions of sea ice concentration, we use the near-real-time data from the Ocean and Sea Ice Satellite Application Facility (OSISAF, Eastwood et al., 2011; http://www.osi-saf.org) from the European Organization for the Exploitation of Meteorological Satellites (EUMETSAT). The data are distributed on a 10 km polar stereographic grid. Because the OSISAF data in the study period are processed with a different algorithm, a hybrid of the Bootstrap algorithm (Comiso, 1986) and the Bristol algorithm (Smith, 1996), and derived from a different passive microwave sensor, SSM/I, on board a different satellite, DMSP F15, the OSISAF dataset can be considered independent of the NSIDC SSMIS dataset.

For further model evaluation, we follow Yang et al. (2014) and compare the model sea ice thickness to independent observations of ice draft provided by the Beaufort Gyre Exploration Project (BGEP) upward-looking sonar (ULS) moorings located in the Beaufort Sea (http://www.whoi.edu/beaufortgyre) and to sea ice thickness data obtained from autonomous ice mass balance (IMB) buoys (Perovich et al., 2013; http://imb.erdc.dren.mil). The error in the ULS measurements of ice draft is about 0.1 m (Melling et al., 1995). Drafts are converted to thickness by multiplying with a factor of 1.1, which is approximately the ratio of the mean seawater (1024 kg/m^3) and sea ice densities (910 kg/m^3) (Nguyen et al., 2011). Note that this simple draft-thickness conversion introduces additional uncertainties due to nonlinearities in

the conversion caused by different ice types, ice densities, and snow loading. These effects are neglected in this study. The IMBs use two acoustic rangefinders to monitor the position of the ice bottom and the snow/ice surface to estimate the sea ice thickness. The accuracy of both sounders is 5 mm (Richter-Menge et al., 2006). The trajectory of the ice mass balance buoy IMB_2011K and the locations of the three moorings BGEP_2011A, BGEP_2011B, and BGEP_2011D are shown in Figure 1. BGEP_2011A and BGEP_2011D are in a region of thin ice during the entire assimilation period. In contrast, BGEP_2011B is in the vicinity of thick ice regimes and partly samples sea ice with thickness of above 1m, where the SMOS data have large errors or are not applicable.

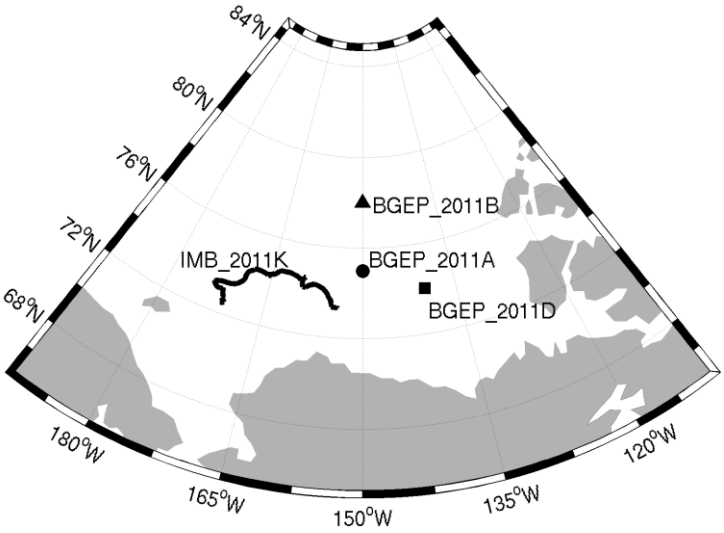

Figure 1. Locations of ULS moorings BGEP_2011A (dot; 74°59.816'N, 149°58.149'W), BGEP_2011B (triangle; 78°0.3950'N, 149°58.462'W) and BGEP_2011D (square; 73°59.649'N, 139°59.043'W), and buoy trajectory from 1 November 2011 to 30 January 2012 of IMB_2011K (black line).

2.4. Data assimilation

For data assimilation, we use the SEIK filter (Pham, 2001) as coded in the Parallel Data Assimilation Framework (PDAF, Nerger and Hiller, 2013; http://pdaf.awi.de). The SEIK filter is a variant of an ensemble-based Kalman filter (Evensen, 1994). It uses an ensemble of model states to estimate the uncertainty in the model state. The data assimilation is performed sequentially by alternating short ensemble forecasts (24 hours in our case) and analysis steps in which the observations are assimilated to correct the ensemble states. In the analysis step, a correction term calculated from deviations between observations and forecast is added to the ensemble averaged

forecast field. In a general form, this can be written as

$$\mathbf{x}^a = \mathbf{x}^f + \boldsymbol{K}\left(\boldsymbol{y} - \boldsymbol{H}\mathbf{x}^{\boldsymbol{f}}\right). \quad (1)$$

Here, $\mathbf{x}^a$ is the analysis field given by the ensemble mean state, $\mathbf{x}^{\boldsymbol{f}}$ is the forecast field, $\boldsymbol{y}$ is the observation, and $\boldsymbol{H}$ is the observation operator, a matrix that extracts the observed part of the model field. The Kalman gain $\boldsymbol{K}$ is calculated by

$$\boldsymbol{K} = \boldsymbol{P}^f\boldsymbol{H}^T(\boldsymbol{H}\boldsymbol{P}^f\boldsymbol{H}^T + \boldsymbol{R})^{-1}, (2)$$

where $\boldsymbol{P}^f$ is the sample covariance matrix of the ensemble and $\boldsymbol{R}$ is the observational error covariance matrix. As an ensemble-based Kalman filter, the SEIK filter uses a computationally efficient formulation of the equations above that avoids storing the full matrix $\boldsymbol{P}^f$ (Evensen, 1994; van Leeuwen and Evensen, 1996). The SEIK filter, however, takes into account that the degrees of freedom for the analysis correction are given by the rank of the ensemble covariance matrix, which is at most the ensemble size minus one, and hence leads to a lower computing cost compared to the ensemble Kalman filter.

Note that the model sea ice thickness is in fact the grid-cell averaged ice thickness, or ice volume divided by the grid-cell area, $\boldsymbol{hc}$, where $\boldsymbol{h}$ is the mean thickness in the ice covered part and $\boldsymbol{c}$ is the fractional ice cover of the grid cell. The observation operator $\boldsymbol{H}$ (eq. 1), extracts $\boldsymbol{c}$ and $\boldsymbol{hc}$ from the model output and maps it to the concentration and thickness data. On the other hand, CryoSat-2 ice thickness data refer to the mean ice thickness of ice covered area. Nevertheless, comparing $\boldsymbol{hc}$ to CryoSat-2 data is mostly uncritical, because the thick sea ice that CryoSat-2 can accurately measure is primarily in 100% ice cover. The SMOS retrieval relies on radiometer measurements and thickness estimates are sensitive also to ice concentration (Tian-Kunze et al., 2014). Therefore, in contrast to CryoSat-2, the SMOS data corresponds to the mean thickness of the whole grid cell, including open water. Thus, comparing to $\boldsymbol{hc}$ is actually appropriate in the marginal ice zone. However, we acknowledge potential uncertainties due to these assumptions.

The LSEIK filter (Nerger et al., 2006) is the localized variant of the SEIK filter. With localization, the filter still applies corrections at each single grid point, but takes into account only observations within a specified radius around the updated grid point. In addition, a quasi-Gaussian weight function (Gaspari and Cohn, 1999) is used to generate the weight of each observation for the analyzed grid point so that

observations are down-weighted with increasing distance from the grid point to be updated (Hunt et al., 2007).

The ensemble-based data assimilation after an ensemble initialization is a sequence of three phases: ensemble forecast; analysis (Eq. 1) given available observations; and ensemble transformation for reinitialization. This sequence is repeated for whenever new data become available.

In the following we detail the LSEIK data assimilation phases and set up for our application:

Time period. The data assimilation is performed with the sea ice-ocean forecasting system from 1 November 2011 to 30 January 2012 assimilating sequentially the observational data and reinitializing the system every 24 hours.

Initialization. To approximate the initial model state error covariance matrix, daily sea ice concentration and grid-cell averaged sea ice thickness snapshots of model integrations from October to December 2011 are collected (resulting in 92 state vectors) and decomposed into empirical orthogonal functions (EOFs) after subtracting the mean state over the integration period (Yang et al., 2015). The ensemble of sea ice concentration and sea ice thickness states are then generated by second-order exact sampling (Pham, 2001). For this, the leading 22 EOFs are multiplied with a random matrix that is constructed given the standard deviation in the set of EOFs and a mean state. The data assimilation system is initialized on 1 November 2011. At this time, the ensemble is generated from the state of the free model run and variance of the EOFs and saved in restart files (one file per ensemble member). The initialization could include more states, for example, from previous years, but each regular analysis step also adds information to the covariance matrix so that in long integrations, the initialization affects the assimilation only in the beginning.

Forecast. The initialized model trajectories evolve in time over the next 24 hours of model integration being forced by an ensemble of 23 UKMO atmospheric 24h forecasts until the next sea ice thickness and/or sea ice concentration observations become available for forecast evaluation and assimilation. During the forecast phase, the ensemble propagates the forecast errors due to uncertainties in the initial conditions and atmospheric forcing. Sea ice or ocean model errors or parameter uncertainties are not considered explicitly (Shlyaeva et al., 2016).

Analysis and reinitialization. Given the observations, the LSEIK computes a corrected state of sea ice concentration and thickness (Eq. 1) and updates the state error covariance matrix estimated from the obtained ensemble of model states. The analysis is carried out for each model grid point given the observations only within the radius of 126 km (~7 grid points). This radius was determined in a parameter study (Yang et al., 2014) to give optimal estimates. After the analysis, the updated fields are written into the model restart files. The model restarts a new forecast from the adjusted restart files and continues the ensemble integration.

2.5. Experimental design

The performance of the forecasting system after including the CryoSat-2 data in the assimilation is investigated in five experiments (Table 1): Exp_Ctrl is a purely prognostic experiment forced by UKMO control forecast fields without any data assimilation. Exp_SSMIS assimilates only SSMIS sea ice concentration data. Exp_SM repeats the experiment by Yang et al. (2016) and assimilates SSMIS sea ice concentration data and SMOS sea ice thickness data. To also constrain thicker sea ice, Exp_SM&CS2 assimilates both SMOS and CryoSat-2 datasets. Exp_CS2SMOS assimilates the combined CS2SMOS data directly. The assimilation of SSMIS sea ice concentration data is also implemented in both Exp_SM&CS2 and Exp_CS2SMOS. In all assimilation experiments, sea ice concentration and thickness form the same state vector and both variables are updated in the analysis step.

Table 1. List of experiments and assimilated datasets

(Data used for assimilation are represented by dots)

Experiments	Sea ice concentration	Sea ice thickness		
	SSMIS	SMOS	CryoSat-2	CS2SMOS
Exp_Ctrl				
Exp_SSMIS	●			
Exp_SM	●	●		
Exp_SM&CS2	●	●	●	
Exp_CS2SMOS	●			●

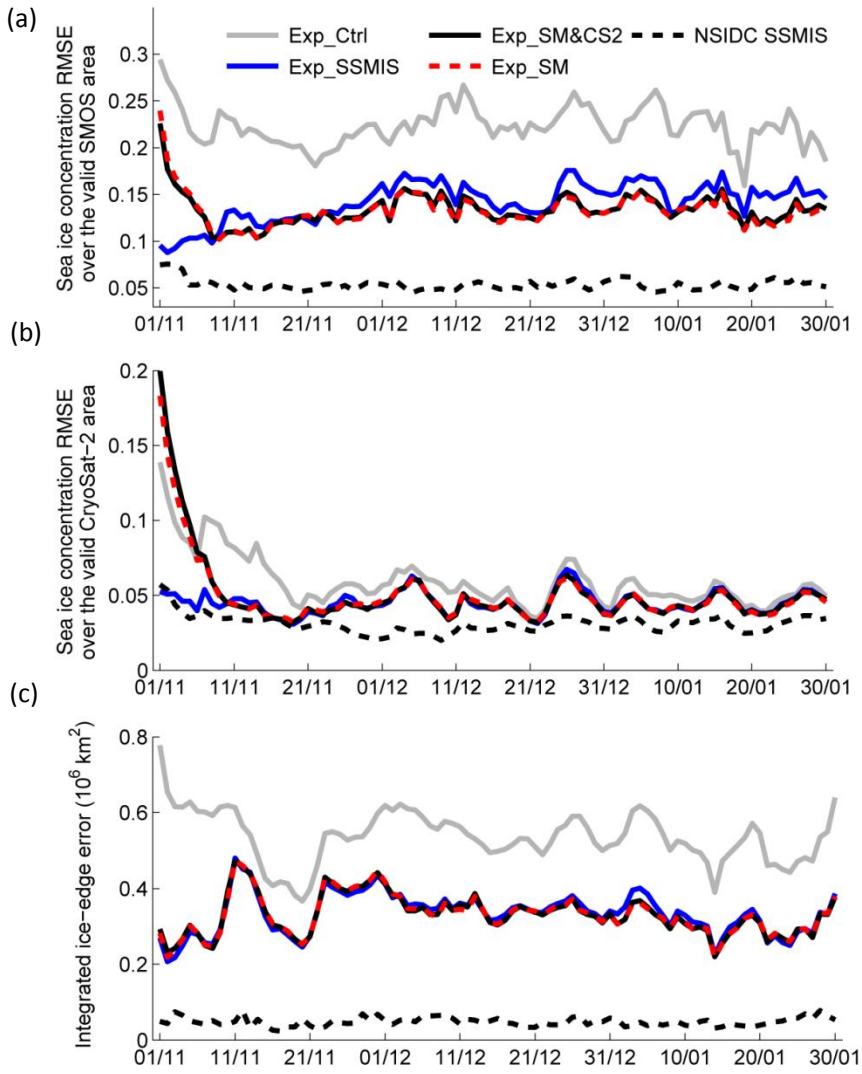

Figure 2. Temporal evolution of (a, b) RMSE with respect to the OSISAF ice concentration data and of (c) the integrated ice-edge error (IIEE) for Exp_Ctrl (grey solid), Exp_SSMIS (blue solid), Exp_SM&CS2 (black solid), Exp_SM (red dashed) and NSIDC SSMIS (black dashed) from 1 Nov 2011 to 30 Jan 2012. Note that subplot (a) is calculated over the valid SMOS area and subplot (b) is calculated over the valid CryoSat-2 area. Date format is dd/mm.

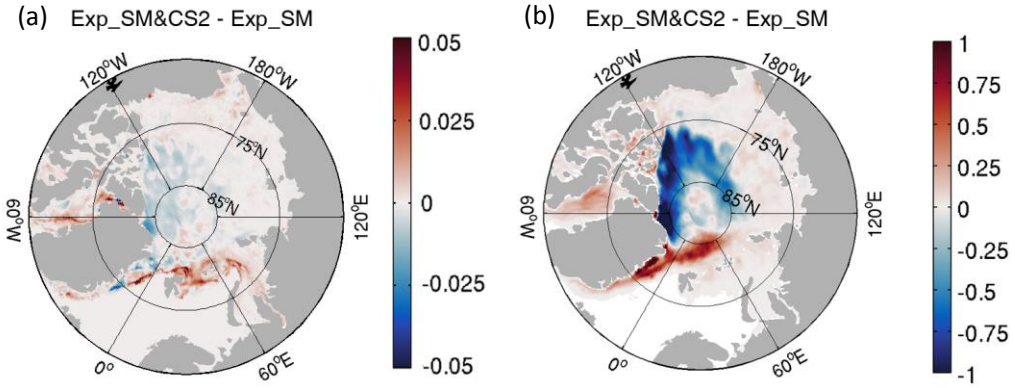

Figure 3. Differences between Exp_SM&CS2 and Exp_SM (a) sea ice concentration and (b) sea ice thickness (m) averaged over 1 Nov 2011 to 30 Jan 2012.

3. **Results**

3.1. Sea ice concentration

To analyze the impact of the data assimilation we examine the mean of the daily ensemble forecast just before the analysis step. For each daily forecast, we follow Yang et al. (2016) and calculate the root-mean-square error (RMSE) of sea ice concentration (ranging from 0 to 1) with respect to the independent OSISAF concentrations, where concentrations are larger than 0.05 in either the model or the observations. During the calculation, the valid SMOS area is where the assimilated SMOS sea ice thickness is below 1.0 m and the valid CryoSat-2 area is where the current weekly CryoSat-2 sea ice thickness is available.

For reference, the RMSEs of NSIDC SSMIS with respect to the OSISAF sea ice concentration data over the valid SMOS and CryoSat-2 area are shown respectively in Figure 2(a, b). Averaged over all three months, the RMSE for the valid SMOS area is 0.053, while it is 0.031 for the valid CryoSat-2 area. It also shows that the RMSE of NSIDC SSMIS over the valid CryoSat-2 area almost reaches the RMSEs of the assimilated model simulations.

Compared to Exp_Ctrl, the assimilation of SSMIS sea ice concentration in Exp_SSMIS, Exp_SM and Exp_SM&CS2 reduces the differences between the forecasts and independent observations (Figure 2(a, b)). The assimilation of sea ice thickness data combined with sea ice concentration data (Exp_SM and Exp_SM&CS2) further reduces the RMSEs with respect to OSISAF data over the valid SMOS data area compared to Exp_SSMIS (Figure 2(a)).

The assimilation of the ice concentration data reduces the mean RMSE by 0.090 in the SMOS data region (Figure 2(a)), but only by 0.009 in the CryoSat-2 data region (Figure 2(b)). This difference is expected because the CryoSat-2 area includes much thicker ice that always coincides with high ice concentration. High ice concentrations limit the potential for sea ice concentration improvements, but sea ice concentration forecasts in the pack are arguably less interesting than in areas of low ice concentration.

The additional assimilation of the CryoSat-2 sea ice thickness (Exp_SM&CS2) does not reduce the RMSE of the sea ice concentration neither over the valid SMOS area nor over the valid CryoSat-2 area. The difference of the mean sea ice concentrations between Exp_SM&CS2 and Exp_SM (Figure 3(a)) shows that the effects of assimilating CryoSat-2 thickness data are small (< 0.05 in concentration) but systematic: assimilating CryoSat-2 slightly decreases the ice concentration in the thick ice area and increases the ice concentration near the ice edge. In areas where there are no thickness data available, the RMSE improves a little (by about 0.01) compared to Exp_SSMIS (Figure not shown).

As an additional metric we use the integrated ice-edge error (IIEE) defined in Goessling et al. (2016). It is computed from counting the area of model grid cells, where the model and satellite data disagree in the presence of sea ice. This metric changes with time, but with after assimilating SSMIS concentration data, the mean IIEE is reduced by approximately 38% (0.204 million km^2) (Figure 2(c)). The assimilation of thickness data does not contribute very much to reducing the IIEE.

Note that assimilating ice thickness leads to larger RMSE during the first 10 days of the experiment (Figure 2(a, b)). This can be explained by the initial thickness bias of Exp_Ctrl that maps into the concentration updates via the covariance between thickness and concentration in the covariance matrix P. The initial concentration bias is generally well below 0.2. The initial thickness has a small bias near the North Pole, but larger biases of easily 1.0 m towards the ice edge and the marginal seas, which is a first-order error. As a consequence, the almost instantaneous adjustment to observed concentration in Exp_SSMIS is slowed down by the thickness bias in experiments Exp_SM and Exp_SM&CS2. For the sea ice thickness, this initial adjustment is not obviously observed as shown in section 3.2 below.

3.2. Sea ice thickness

The RMSE of sea ice thickness is calculated with respect to SMOS and CryoSat-2 sea ice thickness separately over the valid data area of each dataset (Figure 4). Assimilating SSMIS concentration data improves the fit to thickness data only marginally (Figure 4; see also Yang et al., 2014). The improvement is nearly zero for the CryoSat-2 covered area (Figure 4(b)), where ice concentrations are near 1.0 while ice thickness still increases considerably. As a consequence, the covariance between

concentration and thickness is small (Yang et al., 2014). Both Exp_SM and Exp_SM&CS2 improve the sea ice thickness forecasts compared to Exp_Ctrl and Exp_SSMIS. The mean RMSE in the valid SMOS area (Figure 4(a)) reduces from 0.726 m in Exp_Ctrl, to 0.191 m in Exp_SM and 0.236 m in Exp_SM&CS2. Thus, the performance of Exp_SM is better than Exp_SM&CS2 over the thin ice area. This is due to the fact that CryoSat-2 sea ice thickness is sometimes also available in the thin ice area and the RMSE is calculated only with respect to SMOS sea ice thickness. In any case, the difference between Exp_SM and Exp_SM&CS2 is small in the thin ice area. The assimilation of CryoSat-2 data improves the sea ice thickness forecasts in the thick ice area (Figure 4(b)). The mean RMSE reduces from 0.838 m in Exp_Ctrl to 0.653 m in Exp_SM and then 0.383 m in Exp_SM&CS2. The improvement of the thick ice forecast is much larger than the thin ice forecast differences between Exp_SM&CS2 and Exp_SM.

The effect of assimilating CryoSat-2 sea ice thickness in addition to SMOS data is also illustrated in the map of thickness differences (Figure 3(b)). Compared to Exp_SM, Exp_SM&CS2 reduces the ice thickness in the thick ice area and increases the thickness along the sea ice edge from the northeast of Greenland to north of Svalbard. This is consistent with the sea ice thickness observations of CryoSat-2 in these areas. The smaller deviations close to the North Pole stem from missing satellite data.

Figures 5 and 6 show maps of differences between the sea ice thickness estimates of Exp_SM and Exp_SM&CS2 and the assimilated observational datasets SMOS and CryoSat-2. The model-data misfit is smaller in the thin ice area (i.e. compared to SMOS data) for Exp_SM (Figure 5), but for Exp_SM&CS2 the overall agreement with CryoSat-2 data is much better, especially in the thick ice area (Figure 6). That is caused by either no data assimilated in Exp_SM (in thick ice area) or a conflict between the data products in the region east of Greenland and the Baffin Bay. These regions are challenging for satellite remote sensing. In the Fram Strait, ice regimes are characterized by a composite of thinner first-year ice and thicker multiyear ice, rapidly advected southwards. CryoSat-2 data are more trustable here, since SMOS does not register the thick ice. However, certainly at lower latitudes, CryoSat-2 measurements are not repeated daily over the same area. Therefore, uncertainties in

areas of strong ice drift are significant. In the Baffin Bay, sea ice during the freeze-up in autumn is very thin. In addition, the CryoSat-2 product is potentially biased in the Baffin Bay, since the conversion from ice freeboard to thickness (Laxon et al., 2013) is based on a snow climatology that is not well constraint in this area. Therefore, SMOS is more reliable in the Baffin Bay in autumn. On the other hand, in spring, ice thickness can exceed 1.0 m and then also the SMOS ice thickness uncertainty will increase.

To evaluate the performance of the sea ice assimilation experiment Exp_SM&CS2, the 24-hour ice thickness forecasts are compared with independent thickness observations from in situ ULS and IMB buoys (Figure 7). The forecasted ice thicknesses are linearly interpolated from the model grid to the locations of the in situ observations. The assimilation of CryoSat-2 sea ice thickness reduces the overestimation of the thickness at BGEP_2011B (Figure 7(b)), and still maintains the good performance of Exp_SM at the other three locations. The RMSE of Exp_SM&CS2 calculated from daily means at BGEP_2011B is 0.36 m, that of Exp_SM is 0.84 m and that of Exp_Ctrl without assimilation is 1.03 m (Table 2). The assimilation of SSMIS concentration alone (Exp_SSMIS) does not improve the RMSE with the in-situ data over that of the control (Exp_Ctrl) (Table 2). The RMSE of Exp_SM&CS2 and Exp_SM (based on daily means in Table 2) are very similar at BGEP_2011A, BGEP_2011D and IMB_2011K. The considerable improvement of Exp_SM&CS2 compared to Exp_SM at BGEP_2011B is mostly caused by data gaps in the SMOS data for thicknesses larger than 1.0 m. The assimilation of CryoSat-2 sea ice thickness fills these gaps. In the absence of data gaps, Exp_SM and Exp_SM&CS2 are comparable in these specific locations.

In addition, time series of spatially averaged ensemble spread, measured by the ensemble standard deviations (STDs), of 24h ice concentration and thickness forecasts are calculated (Figure not shown). For the ensemble spread of sea ice concentration, only grid points with ice concentration larger than 0.05 are considered. The time series show that similar to Yang et al. (2015), the prior uncertainty modeled by the ensemble of atmospheric forcing results in a stable model ensemble spread after two weeks. The spread represents the posterior model uncertainties which are an implicit part of the forecast.

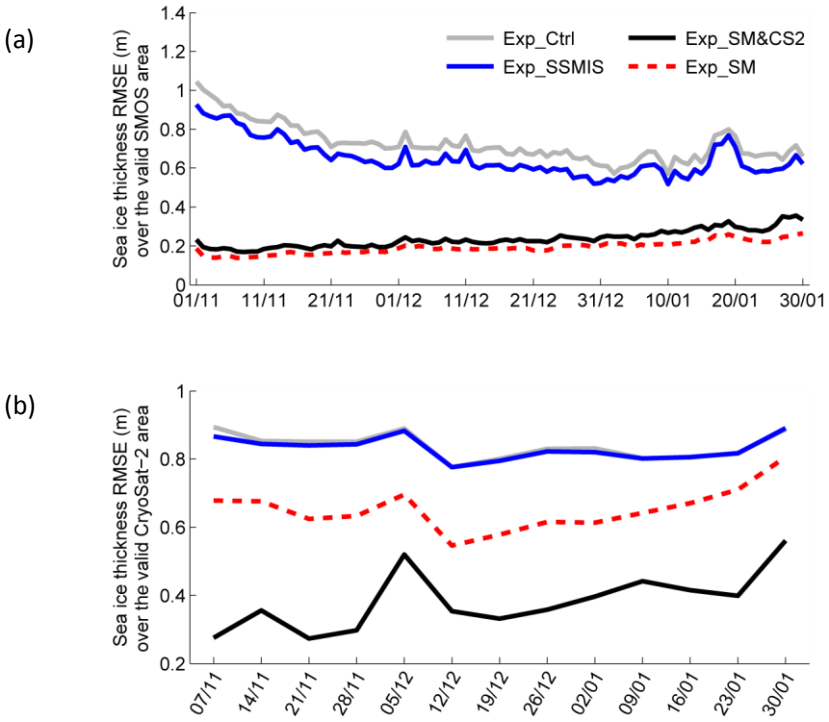

Figure 4. Temporal evolution of RMSE between Exp_Ctrl (grey solid), Exp_SSMIS (blue solid), Exp_SM&CS2 (black solid), Exp_SM (red dashed) and (a) SMOS sea ice thickness (0-1.0 m), (b) CryoSat-2 sea ice thickness from 1 Nov 2011 to 30 Jan 2012. Note that for thickness over the valid CryoSat-2 area (b), the RMSE are computed relative to weekly CryoSat-2 data.

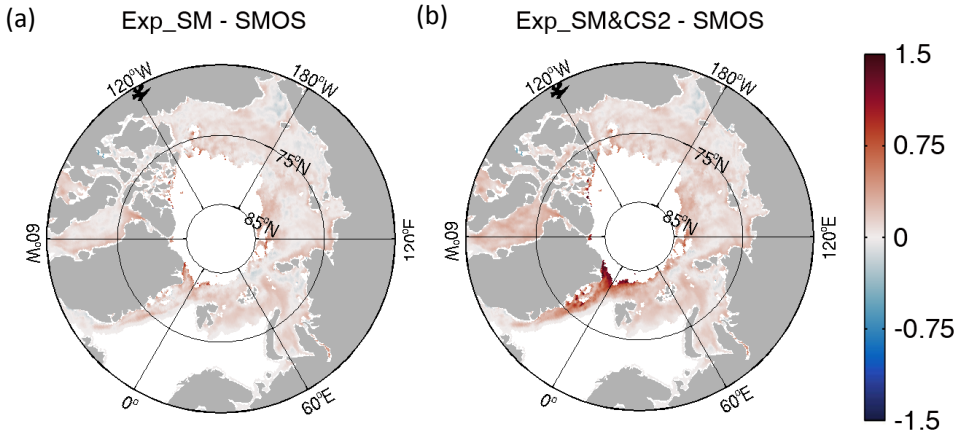

Figure 5. Mean sea ice thickness deviation (m) of (a) Exp_SM and (b) Exp_SM&CS2 from SMOS sea ice thickness averaged from 1 Nov 2011 to 30 Jan 2012.

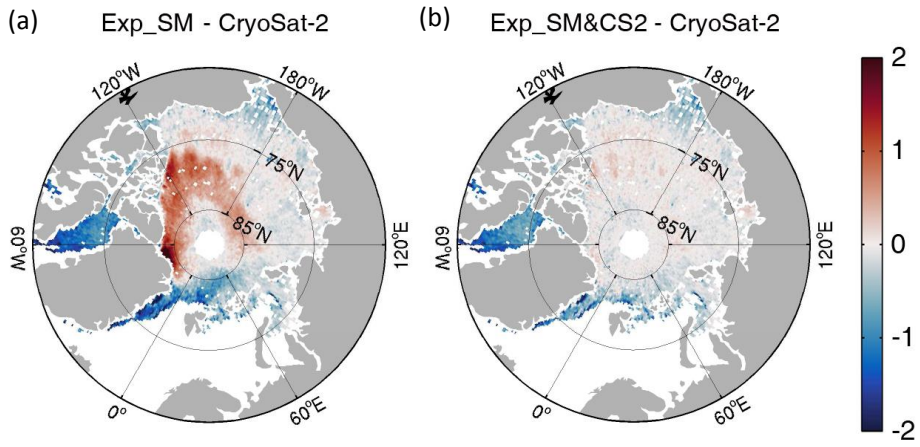

Figure 6. Mean sea ice thickness deviation (m) of (a) Exp_SM and (b) Exp_SM&CS2 from the respective weekly CryoSat-2 sea ice thickness averaged from 1 Nov 2011 to 30 Jan 2012.

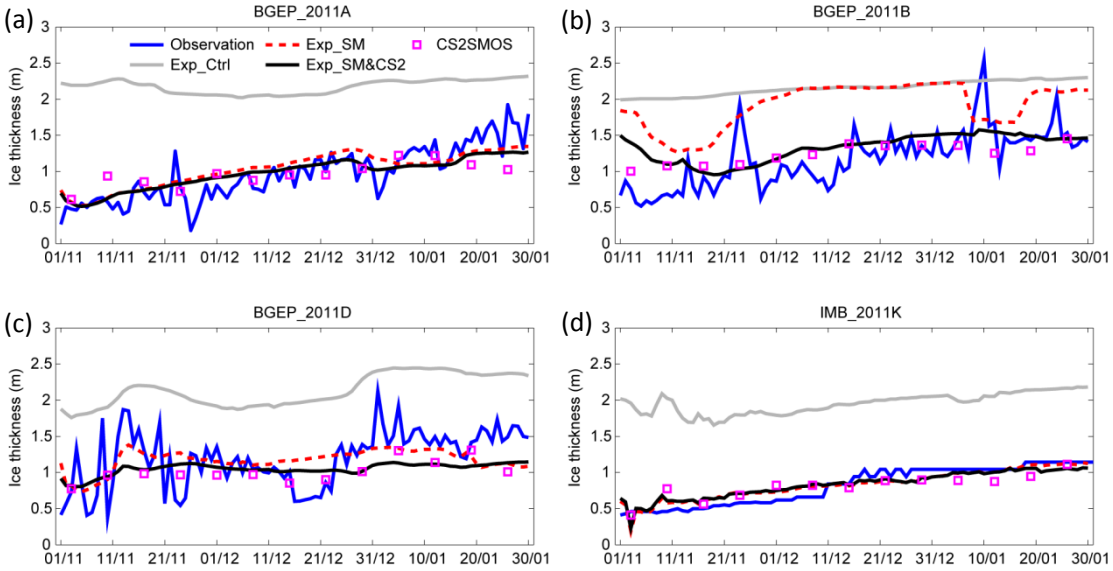

Figure 7. Time series of sea ice thickness (m) at (a) BGEP_2011A, (b) BGEP_2011B, (c) BGEP_2011D, and (d) IMB_2011K from 1 Nov 2011 to 30 Jan 2012. The magenta squares represent weekly CS2SMOS data after they have been linearly interpolated onto the locations of the in situ observations. Note that the errors in measurements are estimated as 0.1 m at BGEP_2011A, BGEP_2011B and BGEP_2011D and 1 cm at IMB_2011K.

Table 2. RMSE (m) between the forecast experiments and the in situ measurements of the ULS moorings BGEP_2011A, BGEP_2011B, and BGEP_2011D, and the IMB buoy IMB_2011K.

Experiment		BGEP_2011A	BGEP_2011B	BGEP_2011D	IMB_2011K
Exp_Ctrl	Daily means	1.26	1.03	0.98	1.15
Exp_SSMIS		1.24	1.05	1.15	1.03
Exp_SM		0.24	0.84	0.35	0.11
Exp_SM&CS2		0.23	0.36	0.38	0.12
CS2SMOS	Weekly means	0.25	0.22	0.28	0.16
Exp_SM&CS2		0.17	0.21	0.29	0.11
Exp_CS2SMOS		0.20	0.23	0.25	0.12

4. The role of model dynamics in data blending

Ricker et al. (2017) exploited the complementary character of SMOS and CryoSat-2 retrievals and combined them with an optimal interpolation into a pan-Arctic sea ice dataset (CS2SMOS). In this section we compare this statistically combined dataset to our Exp_SM&CS2 results, which can be viewed as a dynamically consistent combination of three datasets (SSMIS sea concentration, SMOS and CryoSat-2 sea ice thickness). In this way we can assess the additional information that may be contained in the physics of the sea ice-ocean model in our data assimilation system. Further, we assimilate CS2SMOS directly (Exp_CS2SMOS in Table 1) and compare this to jointly assimilating the separate SMOS and CryoSat-2 datasets in Exp_SM&CS2 (Section 3).

First we compare our Exp_SM&CS2 solution to the CS2SMOS dataset. Mostly, the 3 months mean sea ice thickness difference fields agree within 0.10 m; larger differences above 0.50 m are found mostly in the Chukchi Sea, east of Greenland, and in Baffin Bay, that is, in areas with a fragmented ice cover and individual floes (Figure 8(a)). The weekly CS2SMOS data at the in situ observation points are shown in Figure 7. For CS2SMOS, the RMSEs with respect to those observations are 0.25 m, 0.22 m, 0.28 m and 0.16 m for BGEP_2011A, BGEP_2011B, BGEP_2011D and IMB_2011K, respectively (Table 2). For Exp_SM&CS2, the corresponding RMSEs, which are calculated from weekly means of 24-hour forecasts in order to compare with RMSEs of the weekly CS2SMOS data, are on average lower with 0.17 m, 0.21 m, 0.29 m and 0.11 m (Table 2).

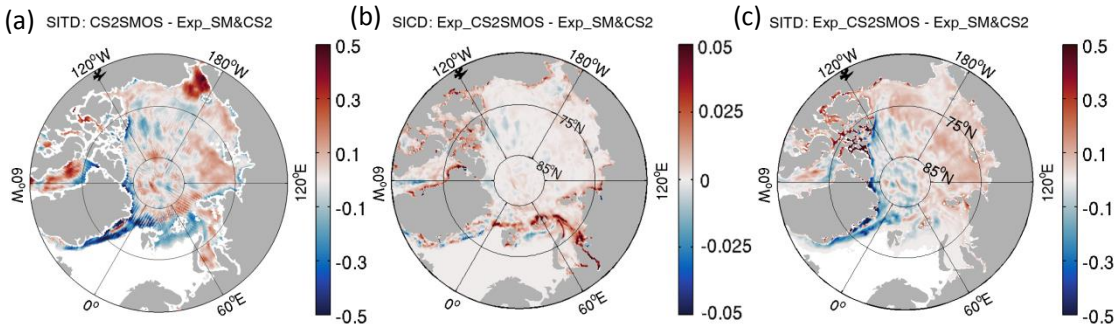

Figure 8. (a) Sea ice thickness difference (SITD) (m) between CS2SMOS and Exp_SM&CS2, (b) sea ice concentration difference (SICD) and (c) sea ice thickness difference (m) between Exp_CS2SMOS and Exp_SM&CS2 averaged from 1 Nov 2011 to 30 Jan 2012. The mean sea ice thickness fields of that time are shown in Figure S1.

When we assimilate the CS2SMOS dataset directly and compare to Exp_SM&CS2 and CS2SMOS, the main differences of sea ice concentration between Exp_CS2SMOS and Exp_SM&CS2 are near the sea ice edge in the marginal ice zone (Figure 8(b)). By comparison, the difference of sea ice thickness in the same marginal ice zones (Figure 8(c)) is smaller than in other areas, mainly because sea ice is so thin in the marginal ice zones that the differences between Exp_CS2SMOS and Exp_SM&CS2 are not visible with the chosen color scale. For Exp_CS2SMOS, the ice is thinner around Greenland and in the Canadian Arctic Archipelago where ice is mostly perennial, but it is thicker over the SMOS data region with mostly thin ice (Figure 8(c)).

The amplitude of the RMSE differences calculated over the valid SMOS area and the valid CryoSat-2 area are below 0.02 for the concentration (Figure 9(a, b)) and below 0.15 m for sea ice thickness (Figure 9(c, d)). For the sea ice concentration fields (Figure 9(a, b)), Exp_SM&CS2 has smaller RMSEs than Exp_CS2SMOS for most of November 2011 to January 2012. For the sea ice thickness forecasts, the RMSEs are smaller for Exp_SM&CS2 over the whole simulation period (Figure 9(c, d)). As the RMSEs in Table 2 show, the Exp_CS2SMOS also has on average larger errors with respect to the in situ observations compared to Exp_SM&CS2.

Generally, the joint assimilation of Exp_SM&CS2 reduces the model-data misfit with respect to OSISAF sea ice concentration and SMOS (< 1.0 m) and CryoSat-2 sea

ice thickness more than assimilating CS2SMOS (Exp_CS2SMOS). Further, in the thickness difference between Exp_CS2SMOS and Exp_SM&CS2 (Figure 8(c)) the strong differences, for example in the Chukchi Sea and in Baffin Bay, are reduced when compared with Figure 8(a), implying that the model rejects the CS2SMOS data where they are inconsistent with the model dynamics. The small thickness differences between Exp_SM&CS2 and SMOS dataset in the Chukchi Sea (less than 0.1 m, Figure 5(b)) support the conclusion that the assimilated solution with model dynamics is more reliable than CS2SMOS alone. These results also demonstrate that the SMOS data have smaller errors in the Chukchi Sea and Baffin Bay during our study period and further are more consistent with the model dynamics.

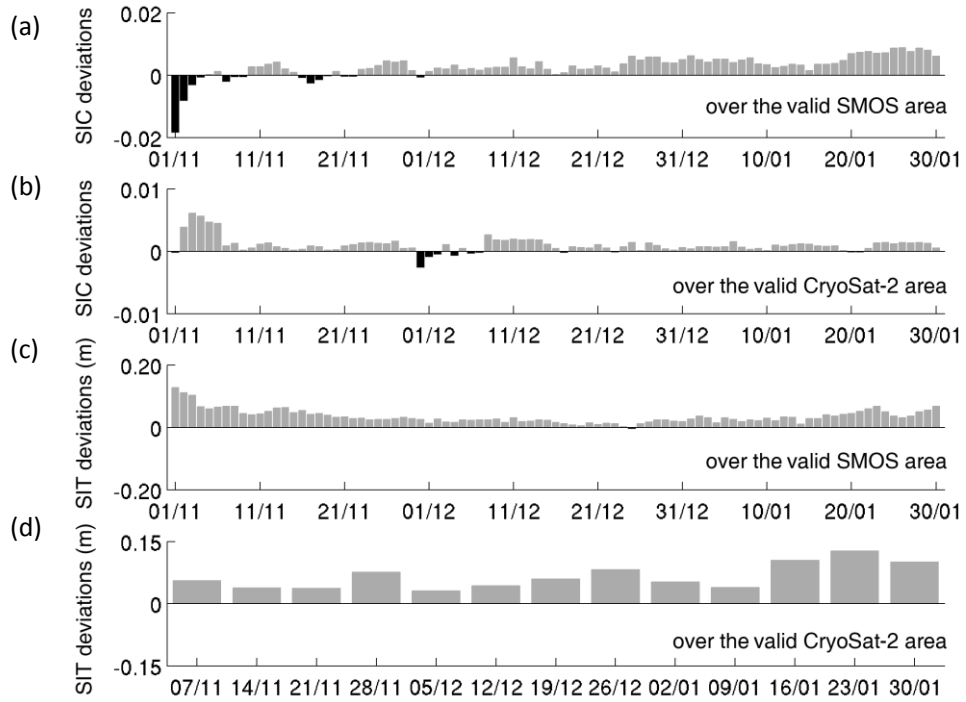

Figure 9. RMSE-differences between Exp_CS2SMOS and Exp_SM&CS2 calculated as RMSE(Exp_CS2SMOS) - RMSE(Exp_SM&CS2), for (a, b) sea ice concentration (SIC) and (c, d) thickness (SIT) (m). The RMSE is calculated over the valid SMOS area for subplot (a) and (c) and over the valid CryoSat-2 area for subplot (b) and (d) in analogy to Figures 2 and 4. The grey bars indicate that RMSE(Exp_CS2SMOS) are larger than RMSE(Exp_SM&CS2), and vice versa for the black bars. Note that for thickness over the valid CryoSat-2 area (d), the RMSE are computed relative to weekly CryoSat-2 data.

5. Conclusions

Exploiting the complementary character of the CryoSat-2 thickness data to that of the SMOS data, a new multi-parameter multi-variate assimilation of thickness and concentration data leads to smaller overall root-mean-square differences with independent data than assimilating only SMOS thickness and SSMIS concentration data. The CryoSat-2 data fill gaps in thick ice regions where SMOS data are unavailable. Our results also suggest that combining thickness and concentration data with an assimilation model provides more reliable thickness estimates than a purely statistical combination where the model dynamics tend to reject unphysical features in the data.

Compared to the model fields without data assimilation, all assimilation experiments show, as expected, considerable improvements of sea ice concentration and sea ice thickness forecasts. The forecasting system needs to spin up for about 10 days before the assimilation of thickness leads to consistent sea ice concentration improvements. The simultaneous assimilation of CryoSat-2 and SMOS sea ice thickness data does not significantly improve the sea ice concentration compared to assimilating the thin-ice data from SMOS alone, but the model agrees better with in-situ thickness data when the ice is thick and still maintains the good agreement with in situ thickness observations when the ice is thin. The small effect on ice concentration can be explained by the fact that the sea ice concentration in thick multi-year ice regions is always close to 100% during the cold season. The effects on thick ice show that the perennial sea ice thickness cannot be corrected by assimilating only the SMOS sea ice thickness data, because it provides reliable thickness estimates only for ice thicknesses below 1.0 m.

Compared to the assimilation of the statistically combined CS2SMOS dataset, we found that the joint assimilation of SMOS and CryoSat-2 results in smaller RMSEs over most of the simulation period. This suggests that our assimilation system with SMOS and CryoSat-2 thickness data allows extra model information to positively affect the simulated sea ice thickness. Both, the joint assimilation of SMOS and CryoSat-2 data and the assimilation of CS2SMOS lead to smaller errors in the Chukchi Sea than in the CS2SMOS data product. This suggests that the model dynamics play an important role in the assimilation and have the potential to reduce bias in satellite retrievals. However, our analysis is limited by sparse in-situ data and

their corresponding uncertainties, so that longer simulation periods that span more in-situ data are required to improve the validation analysis in the future.

This work is a step towards our final goal of establishing a sea ice-ocean forecasting system with multi-variate data assimilation for the daily, weekly (Yang et al., 2015), sub-seasonal (Yang et al., 2014) or even seasonal (Day et al., 2014) Arctic sea-ice prediction as well as for further general investigation of the Arctic variability. The 3-month integration and relatively localized in situ observations are not sufficient for a robust validation of the entire Arctic. Nevertheless, we have shown the potential for generating a sea ice thickness reanalysis dataset. The next step is to extend the study period to the time covered by the thickness datasets. This will give access to more verification datasets and will let us explore the performance of the system in summer months when only ice concentration data are available. In the absence of thickness data in summer, we still expect some success also for the thickness fields, because sea ice thickness can be corrected by the assimilation of sea ice concentration due to the good correlations between sea ice concentration and thickness in summer. The influence of the assimilation on the ocean state and the snow thickness as well as accounting for uncertainties in internal sea ice model parameters (Shlyaeva et al., 2016) are subjects for future research. Additional data, such as near real-time sea ice drift data (e.g., Lavergne et al., 2010) or sea surface temperature, will be assimilated to better constrain the model.

Acknowledgements

We thank the University of Hamburg for providing SMOS sea ice thickness data, National Snow and Ice Data Center (NSIDC) and the OSISAF High Latitude Processing Center for the ice concentration data, the Woods Hole Oceanographic Institution for the sea ice draft data, the Cold Regions Research and Engineering Laboratory for IMB data, and the European Centre for Medium-Range Weather Forecasts for the UKMO ensemble forecasting data. This study is supported by the BMBF (Federal Ministry of Education and Research, Germany) and SOA (State Oceanic Administration, China) joint project (01DO14002) and the National Natural Science Foundation of China (41376005, 41376188). We also thank the three anonymous reviewers for their valuable suggestions.

References

Bougeault P, Toth Z, Bishop C, Brown B, Burridge D, Chen DH, Ebert B, Fuentes M, Hamill TM, Mylne K, Nicolau J, Paccagnella T, Park YY, Parsons D, Raoult B, Schuster D, Dias PS, Swinbank R, Takeuchi Y, Tennant W, Wilson L, Worley S. 2010. The THORPEX Interactive Grand Global Ensemble. *Bull. Am. Meteorol. Soc*. **91**(8): 1059–1072, doi:10.1175/2010BAMS2853.1.

Bowler NE, Arribas A, Mylne KR, Robertson KB, Beare SE. 2008. The MOGREPS short-range ensemble prediction system. *Q. J. R. Meteorol. Soc*. **134**(632): 703–722, doi:10.1002/qj.234.

Brodzik MJ, Billingsley B, Haran T, Raup B, Savoie MH. 2012. EASE-Grid 2.0: Incremental but Significant Improvements for Earth-Gridded Data Sets. *ISPRS Int. J. Geo-Information*. **1**(3): 32–45, doi:10.3390/ijgi1010032.

Castro-Morales K, Kauker F, Losch M, Hendricks S, Riemann-Campe K, Gerdes R. 2014. Sensitivity to realistic ice thickness distributions and snow parameterizations of simulated Arctic sea ice. *J. Geophys. Res*. **119**: 1–13, doi:10.1002/2013JC009342.

Cavalieri DJ, Parkinson CL, DiGirolamo N, Ivanoff A. 2012. Intersensor calibration between F13 SSMI and F17 SSMIS for global sea ice data records. *IEEE Trans. Geosci. Remote Sens*. **9**: 233 – 236.

Comiso JC. 1986. Characteristics of Arctic winter sea ice from satellite multispectral microwave observations. *J. Geophys. Res*. **91**: 975–994, doi:10.1029/JC091iC01p00975.

Day JJ, Hawkins E, Tietsche S. 2014. Will Arctic sea ice thickness initialization improve seasonal forecast skill? *Geophys. Res. Lett*. **41**: 7566–7575, doi:10.1002/2014GL061694.

Eastwood S, Larsen KR, Lavergne T, Neilsen E, Tonboe R. 2011. OSI SAF global sea ice concentration reprocessing: product user manual, version 1.3. EUMETSAT OSI SAF (Product 0SI-409).

Evensen G. 1994. Sequential data assimilation with a non-linear quasi-geostrophic model using Monte-Carlo methods to forecast error statistics. *J. Geophys. Res*. **99**: 10143–10162, doi:10.1029/94JC00572

Gaspari G, Cohn SE. 1999. Construction of correlation functions in two and three dimensions. *Q. J. Roy. Meteor. Soc*. **125**: 723–757.

Goessling HF, Tietsche S, Day JJ, Hawkins E, Jung T. 2016. Predictability of the Arctic sea ice edge. *Geophys. Res. Lett*. **43**(4): 1642–1650.

Hibler W III. 1979. A dynamic thermodynamic sea ice model. *J. Phys. Oceanogr*. **9**(4): 815–846

Hibler W III. 1984. `The role of sea ice dynamics in modeling CO2 increases`. In *Climate Processes and Climate sensitivity.* American Geophysical Union: Washington, D. C.; pp 238–253, doi: 10.1029/GM029p0238.

Hunt BR, Kostelich EJ, Szunyogh I. 2007. Efficient data assimilation for spatiotemporal chaos: A local ensemble transform Kalman filter. *Phys. D Nonlinear Phenom*. **230**(1–2): 112–126, doi:10.1016/j.physd.2006.11.008.

Janjić T, Bormann N, Bocquet M, Carton JA, Cohn SE, Dance SL, Losa SN, Nichols NK, Potthast R, Waller JA, P. Weston P. 2017. On the representation error in data assimilation. *Q. J. R. Meteorol. Soc.* (in press)

Lavergne T, Eastwood S, Teffah Z, Schyberg H, Breivik LA. 2010. Sea ice motion from low - resolution satellite sensors: An alternative method and its validation in the Arctic. *J. Geophys. Res*. **115**: C10032, doi:10.1029/2009JC005958.

Laxon SW, Giles KA, Ridout AL, Wingham DJ, Willatt R, Cullen R, Kwok R, Schweiger A, Zhang J, Haas C, Hendricks S, Krishfield R, Kurtz N, Farrell S, Davidson M. 2013. CryoSat-2 estimates of Arctic sea ice thickness and volume. *Geophys. Res. Lett*. **40**(4): 732–737, doi:10.1002/grl.50193.

Lindsay RW, Zhang J. 2006. Assimilation of Ice Concentration in an Ice–Ocean Model. *J. Atmos. Ocean. Technol*. **23**(5): 742–749, doi:10.1175/JTECH1871.1.

Lisæter KA, Evensen G, Laxon SW. 2007. Assimilating synthetic CryoSat sea ice thickness in a coupled ice-ocean model. *J. Geophys. Res. Ocean*. **112**(7): 1–14, doi:10.1029/2006JC003786.

Lisæter KL, Rosanova J, Evensen G. 2003. Assimilation of ice concentration in a coupled ice-ocean model, using the Ensemble Kalman filter. *Ocean Dyn*. **53**(4): 368–388, doi:10.1007/s10236-003-0049-4.

Losch M, Menemenlis D, Campin JM, Heimbach P, Hill C. 2010. On the formulation of sea ice models. Part 1: Effects of different solver implementations and parameterizations. *Ocean Model*. **33**(1–2): 129–144, doi:10.1016/j.ocemod.2009.12.008.

Marshall J, Adcroft A, Hill C, Perelman L, Heisey C. 1997. A finite-volume, incompressible Navier Stokes model for studies of the ocean on parallel computers. *J. Geophys. Res*. **102**: 5753–5766, doi:10.1029/96JC02775.

Massonnet F, Mathiot P, Fichefet T, Goosse H, Konig Beatty C, Vancoppenolle M., Lavergne T. 2013. A model reconstruction of the Antarctic sea ice thickness and volume changes over 1980–2008 using data assimilation. *Ocean Modell*. **64**: 67–75, doi:10.1016/j.ocemod.2013.01.003.

Melling H, Johnston PH, Riedel D. 1995. Measurements of the Underside Topography of Sea Ice by Moored Subsea Sonar. *J. Atmos. Ocean. Technol*. **12**(3): 589–602.

Menemenlis D, Campin JM, Heimbach P, Hill C, Lee T, Nguyen A, Schodlok M, Zhang H. 2008. ECCO2: High resolution global ocean and sea ice data synthesis. *Mercat. Ocean Q. Newsl*. **31**: 13–21.

Mu L, Zhao J, Zhong W. 2017. Regime shift of the dominant factor for halocline depth in the Canada Basin during 1990–2008. *Acta Oceanol. Sin*. **36**(1): 35–43, doi:10.1007/s13131-016-0883-0.

Nerger L, Danilov S, Hiller W, Schröter J. 2006. Using sea-level data to constrain a finite-element primitive-equation ocean model with a local SEIK filter. *Ocean Dynamics*. **56**(5/6): 634–649.

Nerger L, Hiller W. 2013. Software for ensemble-based data assimilation systems-Implementation strategies and scalability. *Comput. Geosci*. **55**: 110–118, doi:10.1016/j.cageo.2012.03.026.

Nguyen AT, Menemenlis D, Kwok R. 2011. Arctic ice-ocean simulation with optimized model parameters: Approach and assessment. *J. Geophys. Res. Ocean*. **116**(4): 1–18, doi:10.1029/2010JC006573.

Park YY, Buizza R, Leutbecher M. 2008. TIGGE: Preliminary results on comparing and combining ensembles. *Q. J. R. Meteorol. Soc*. **134**(637): 2029–2050, doi:10.1002/qj.334.

Parkinson CL, Washington WM. 1979. A large-scale numerical model of sea ice. *J. Geophys. Res*. **84**(C1):311–337.

Perovich DK, Richter-Menge JA, Elder B, Arbetter T, Claffey K, Polashenski C. 2013. Observing and understanding climate change: Monitoring the mass balance, motion, and thickness of Arctic sea ice. http://imb.erdc.dren.mil/.

Pham DT. 2001. Stochastic Methods for Sequential Data Assimilation in Strongly Nonlinear Systems. *Mon. Weather Rev*. **129**(5): 1194–1207, doi:10.1175/1520-0493(2001)129<1194:SMFSDA>2.0.CO;2.

Pham DT, Verron J, Gourdeau L. 1998. Singular evolutive Kalman filters for data assimilation in oceanography. *C. R. Acad. Sci. Paris, Earth Planet. Sci*. **326**: 255–260.

Richter-Menge JA, Perovich DK, Elder BC, Claffey K, Rigor I, Ortmeyer M. 2006. Ice mass-balance buoys: A tool for measuring and attributing changes in the thickness of the Arctic sea ice cover. *Annals of Glaciology*. **44**: 205–210.

Ricker R, Hendricks S, Helm V, Skourup H, Davidson M. 2014. Sensitivity of CryoSat-2 Arctic sea ice freeboard and thickness on radar-waveform interpretation. *Cryosphere*. **8**(4): 1607–1622, doi:10.5194/tc-8-1607-2014.

Ricker R, Hendricks S, Kaleschke L, Tian-Kunze X, King J, Haas C. 2017. A weekly Arctic sea-ice thickness data record from merged CryoSat-2 and SMOS satellite data. *The Cryosphere*. **11**: 1607–1623, doi: 10.5194/tc-11-1607-2017.

Shlyaeva A, Buehner M, Caya A, Lemieux J-F, Smith GC, Roy F, Dupont F, Carrieres T. 2016. Towards ensemble data assimilation for the Environment Canada Regional Ice Prediction System. *Q.J.R. Meteorol. Soc*. **142**: 1090–1099, doi:10.1002/qj.2712.

Smith DM. 1996. Extraction of winter total sea-ice concentration in the Greenland and Barents Sea from SSM/I data. *Int. J. Remote Sens*. **17**: 2625–2646, doi: 10.1080/01431169608949096.

Smith WH, Sandwell D. 1997. Global Sea Floor Topography from Satellite Altimetry and Ship Depth Soundings. *Science*. **277**(5334): 1956–1962, doi:10.1126/science.277.5334.1956.

Stark JD, Ridley J, Martin M, Hines A. 2008. Sea ice concentration and motion assimilation in a sea ice-ocean model. *J. Geophys. Res. Ocean*. **113**(5), doi:10.1029/2007JC004224.

Tian-Kunze X, Kaleschke L, Maaß N, Mäkynen M, Serra N, Drusch M, Krumpen T. 2014. SMOS-derived thin sea ice thickness: Algorithm baseline, product specifications and initial verification. *The Cryosphere*. **8**(3): 997–1018, doi:10.5194/tc-8-997-2014.

Tilling RL, Ridout A, Shepherd A, Wingham DJ. 2015. Increased Arctic sea ice volume after anomalously low melting in 2013. *Nat. Geosci*. **8**(8): 643–646, doi:10.1038/ngeo2489.

van Leeuwen PJ, Evensen G. 1996. Data assimilation and Inverse methods in terms of a Probabilistic Formulation. *Mon. Weather Rev*. **124**: 2898-2913, doi: 10.1175/1520-0493(1996)124<0085:AOGADF>2.0.CO;2.

Wingham DJ, Francis CR., Baker S, Bouzinac C, Brockley D, Cullen R, Chateau-Thierry P, Laxon SW, Mallow U, Mavrocordatos C, Phalippou L, Ratier G, Rey L, Rostan F, Viau P., Wallis DW. 2006. CryoSat: A mission to determine the fluctuations in Earth's land and marine ice fields. *Adv. Sp. Res.* **37**(4): 841–871, doi:10.1016/j.asr.2005.07.027.

Xie J, Counillon F, Bertino L, Tian-Kunze X, Kaleschke L. 2016. Benefits of assimilating thin sea ice thickness from SMOS into the TOPAZ system. *The Cryosphere*. **10**: 2745–2761, doi:10.5194/tc-10-2745-2016.

Yang Q, Losa SN, Losch M, Tian-Kunze X, Nerger L, Liu J, Kaleschke L, Zhang Z. 2014. Assimilating SMOS sea ice thickness into a coupled ice-ocean model using a local SEIK filter. *J. Geophys. Res. Ocean*. **119**(10): 6680–6692, doi:10.1002/2014JC009963.

Yang Q, Losa SN, Losch M, Jung T, Nerger L. 2015. The role of atmospheric uncertainty in Arctic summer sea ice data assimilation and prediction. *Q. J. R. Meteorol. Soc*. **141**(691): 2314–2323, doi:10.1002/qj.2523.

Yang Q, Losch M, Losa SN, Jung T, Nerger L. 2016. Taking into account atmospheric uncertainty improves sequential assimilation of SMOS sea ice thickness data in an ice-ocean model. *J. Atmos. Ocean. Technol*. **33**(3): 397–407, doi:10.1175/JTECH-D-15-0176.1.

Zhang J, Hibler W III. 1997. On an efficient numerical method for modeling sea ice dynamics. *J. Geophys. Res*. **102**(C4): 8691–8702, doi: 10.1029/96JC03744

Zhang J, Hibler W III, Steele M, Rothrock DA. 1998. Arctic ice-ocean modeling with and without climate restoring. *J. Phys. Oceanogr*. **28**: 191–217.